Three-dimensional computer reconstruction of the airway- and the vascular systems of the lung of the domestic fowl, *Gallus gallus* variant *domesticus*

Jeremy D. Woodward[1], Yolanda Ramonisi[2], Reatlegile Mashiteng[2], Lolo Mokae[2], John N. Maina[2]

[1]Division of Medical Biochemistry and Structural Biology, Structural Biology Research Unit, University of Cape Town, Observatory 7925, South Africa.
[2]Department of Zoology, University of Johannesburg, Auckland Park, Johannesburg 2006, South Africa.

Corresponding and presenting author: jmaina@uj.ac.za

Abstract

Invariably, any type of microscopic imaging modality can be used to reconstruct morphological data in three-dimensions (3-D). These techniques allow us to study the structural characteristics of cells, tissues and organs and gaining meaningful insights into their form and function. One of the oldest methods for studying biological entities in 3-D is serial histological-section reconstruction (SHSR) which dates back to the late 19th century. Despite the advent of competing modern techniques that are faster, cheaper and easier to apply and that work in an automated fashion, this method (SHSR) remains indispensable. It is because reconstructions resulting from sections generally display better contrast and signal-to-noise ratio. Additionally, dyes and labels can be used more effectively when applied to the surfaces of sections than to, e.g., resin sample blocks: functional units can therefore be identified by coloured- or fluorescent signals. SHSR is useful from ~0.2 µm resolution and can easily sample large volumes in the 1000^3 voxel range. These characteristics make it particularly effective for preparing accurate, high-resolution 3-D representations of micro-anatomical data. Here, we report on computational use of SHSR in investigation of the structure of the airway- and vascular systems of the mature lung of the domestic fowl, *Gallus gallus* variant *domesticus*. The topographical relationships between the structures were thoroughly examined after preparation of movies that allowed us to rotate the reconstruction around different axes and extract and re-insert different parts back into the visualization. In the extant air-breathing vertebrates, the avian respiratory system (the lung-air sac system) is structurally the most complex and functionally the most efficient. Its unique design largely explains how, among only a few other extant animal taxa, birds attained volancy. Powered (active) flight is an exceptionally energetically costly mode of locomotion which requires large amounts of oxygen to sustain. While it has been continuously studied for over the last four centuries, some aspects of the structure and function of the avian lung remain uncertain and contentious. They include the airflow dynamics across the lung, the arrangement of the airway- and vascular systems and the shapes, sizes and spatial organization of the terminal respiratory units. We noted that in contrast to the mammalian lung, where arterial- and airway systems track each other and the venous system runs segmentally, i.e., between the other two systems, in the avian lung, the corresponding structures do not display similar close following. This may be explained by the unique development and evolution of the avian lung: two morphologically- and functionally distinct parts, namely the paleopulmo and the neopulmo, exist. The parts develop at different times which later combine into one organ. It explains how and why the airways- and the blood vessels do not track and even pattern each fundamentally because the conduits are dedicated to the distinctive parts of the lung with which they were associated.

Introduction

A number of techniques are available to generate volumetric ultrastructural models, and combination of a variety of strategies is now possible for tailoring to specific biological questions and applications. [1]

Through the process of evolution by natural selection [2], living things develop in specific ways to enable them to best execute functions. Understanding cellular dynamics and processes is fundamental to characterizing the underpinnings of life. Most diseases and pathologies arise from cellular abnormalities which trigger intracellular biochemical changes. After the invention of the compound light microscope, some four-and-half centuries ago by Zacharias Jansen (1580-1638) in 1595 [3] [4] and for nearly three hundred years thereafter, microscopic study of biological structures was limited to two-dimensional (2-D) delineation, depiction and description. In the late 19th century, researchers desiring to understand the three-dimensional (3-D) attributes of biological entities employed different ingenious visualization aids to examine serial sections, such as projecting lines from the outlines of structures to produce an image of the object perpendicular to the direction of sectioning [5] or by tracing outlines of the object of interest onto stacks of glass sheets [6] [7]. Modifications on these types of techniques were still being used [8] when Sydney Brenner first applied computers to the problem of visualizing serial section reconstructions in the early 1970's [9]. More recently however, advances in computing power; software; imaging technology as well as visualization tools have spurred the development of a large number of 3-D reconstruction approaches. These techniques are revolutionizing the fields of molecular-, cellular- and tissue biology [1] [10]-[21]: even four-dimensional (4-D) preparations or visualizations are now possible [21]-[23]. The distinctive functions that are displayed by biological structures stem from a multitude of minute physical and biochemical events than occur between and among topologically connected structural components at the different levels of the organization of highly complex assemblages [24]. The spatial conformation (shape) of the structural components that comprise living matter is ubiquitously 3-D [25]-[28]. Recently, 3-D cell- and organoid culture have become particularly popular in studies of cell development, morphology, differentiation, host-pathogen interaction and effects of drug treatments compared to the traditional 2-D ones [23] [29]-[41]. It has been recognized that cells which are cultured in 3-D cell culture assays behave utterly differently compared to those 'grown' in 2-D ones [31] [32]. Comparative investigations have indicated that 2-D cell cultures lose tissue distinctive assemblage, generating changes in mechanical and biochemical signals and disrupting cell-cell or cell matrix connections [31]. In drug delivery studies, while many preparations may show success in 2-D cell cultures, this is not the case in *in vivo* studies because the 3-D environment of the large number of cells in the body may render it problematical for the drugs to equally affect all cells [30]. Furthermore, although in 2-D culture cells acquire a spheroid morphology, the clusters are formed mainly by aggregation of cell masses instead of dividing from a single cell and the groupings of cells are significantly larger than those obtained by 3-D culture [36]. 3-D cell culture optimally supports the 3-D shape of cells, thereby providing a physiologically appropriate environment similar to the one which exists in the living tissue [34]-[36]. It is by coiling and folding into proper 3-D shape that proteins can perform their complex biochemical function(s). Here, two examples are given to underscore the importance of 3-D configuration in proper function of biological components.

In microscopic biology, 3-D reconstruction is a highly instructive investigative technique [18] [42]-[45]. It involves constructing a spatial model of a biological entity from a sufficient

number of 2-D images [46]-[48]. Unfortunately, because of the high cost of time and materials as well as the special skills required to perform it, 3-D reconstruction has not been employed in morphological studies as much as it should have been. The 2-D images needed to prepare the 3-D shape can be acquired by manual preparation of serial sections or by tomographic methods using any measureable signal that is able to penetrate the specimen such as: light, ultrasound, gamma rays, X-rays, neutrons or electrons [18] [49]-[52]. Serial section 3-D reconstruction is the oldest method of obtaining 3-D spatial micro-anatomical data and dates back to the late 19th century [53]-[55]. Recent advances in optical microscopical sectioning techniques as well as automatic block-face image capturing methods like episcopic fluorescence image capturing (EFIC) or surface imaging microscopy (SIM) [56] [57] have considerably increased the efficiency and the accuracy of serial sectioning. Regarding possible sub-micron resolution, compared to the modern 3-D reconstruction techniques, conventional light microscopical (histological) sections have certain advantages of which the main ones are contrast and large sample size which is investigated [11] [18] [58] [59]. Only a few state-of-the-art 3-D reconstruction techniques, e.g., synchrotron-based microcomputer tomography (µCT) or focused ion beam scanning electron microscopy (FIB/SEM) tomography compare in resolution with imaging sections [60]. As more robust ways of utilizing 3-D reconstruction technology continue to be developed, 3-D imaging and animation will constitute an indispensable investigative arsenal in the morphologist's toolbox. Old questions will be revisited and investigated from different perspectives and new questions will be formulated and researched. 3-D reconstruction has lately found application in new research fields such as tissue engineering and regenerative medicine [60]-[63].

In this investigation, we have performed 3-D computer reconstruction on serial histological sections to study the spatial arrangement of the airway- and the vascular systems of a bird's (avian) lung. Among the extant air-breathing vertebrates, the avian respiratory system (the lung-air sac system) is structurally the most complex and functionally the most efficient [64]-[72] compared with the mammalian one. Although it has been continuously investigated for well over four centuries (i.e., since [73]), still, some important aspects of its biology remain unclear and/or controversial [74]. Like the invaginated gas exchangers of other vertebrates, the lungs of birds are ventilated tidally, i.e., in-and-out, and in addition the avian lung (specifically the paleopumonic part of it) is ventilated unidirectionally and continuously in a caudocranial direction, i.e., back-to-front. This is achieved by synchronized bellows-like actions of the air sacs. The path followed by the inspired air across the avian lung is controlled by aerodynamic valving [75] and not by anatomical valves or sphincters, as it was once believed. Morphometrically, the avian lung has thin blood-gas barrier, large respiratory surface area and large blood capillary volume, structural parameters which confer an exceptionally high pulmonary diffusing capacity for oxygen [71] [76]-[78]. Such specializations explain why except for bats, birds are the only other vertebrate animals that have attained powered (active) flight which is an energetically highly costly form of locomotion which requires particular specializations [79]. Some birds can fly nonstop over long distances and others fly under the extreme hypoxic conditions of the high altitude [78]-[82]. Here, we present a 3-D reconstruction method for multi-view image acquisition of microscopic samples combined with pre- and post-processing steps including correlation-based image registration, filtering and a combination of manual and automated segmentation.

Materials and methods

Fixation and processing of the lung

The Animal Ethics Committee of the University of Johannesburg approved all experimental procedures (Clearance Number: 2017-06-29/Maina). A mature domestic fowl (chicken), *Gallus gallus* variant *domesticus*, was killed by intravenous injection with pentobarbitone sodium (Euthanase®) into the brachial vein at a dosage of 2mg/kg. Thereafter, the lungs were fixed by intratracheal instillation of phosphate buffered 2.5% glutaraldehyde (350 mOsm L^{-1}, pH 7.4) at a pressure head of 3 kPa. The trachea was ligated and the fixative left *in situ* for six hours. Afterwards, the lungs were carefully dissected out from their costal attachments. Whole lungs were processed and embedded in paraffin wax according to routine histological procedures.

Serial sectioning and imaging

Two-thousand six hundred and eighty-nine (2689) transverse serial sections were cut at 8 µm thickness, stained with haematoxylin and eosin and mounted onto glass slides. The whole series of sections constituted the entire lung volume. A total of thirty seven (37) sections were lost or damaged during sectioning. The rest were mounted onto glass slides. In most cases, the lost sections were non-consecutive, but in one case nine sections (72 µm) were lost in a row. An area measuring 12.88 × 9.655 mm, which included the entire transverse section through the lung was photographed using an Axioskop image analyser (Zeiss Instruments) at a magnification of x10 in uncompressed Tiff image format at a resolution of 2576 × 1931 pixels with a calibrated sampling of 5 µm/pixel.
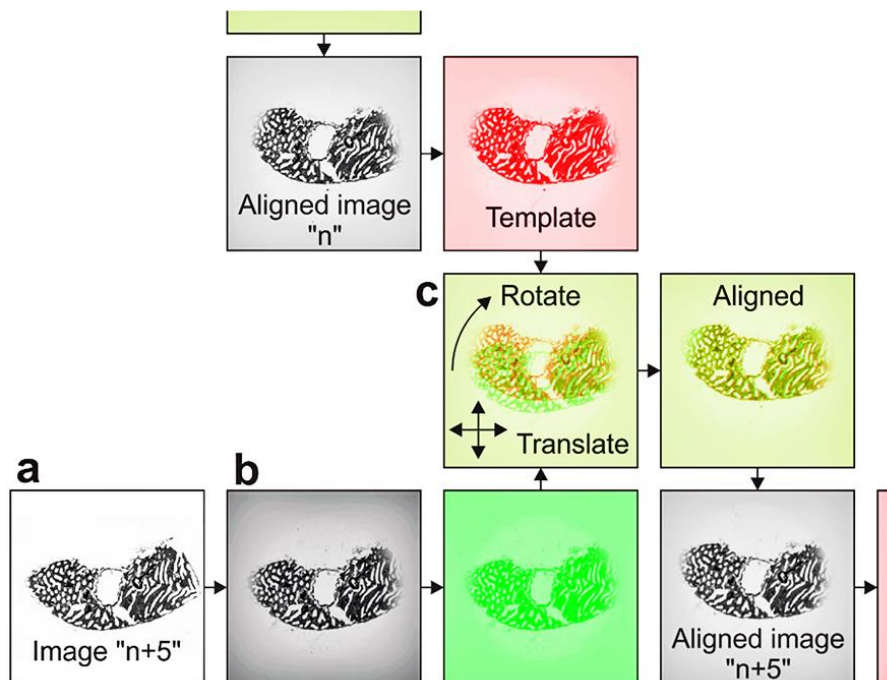
Figure 1: Image processing and alignment. (a). Every 5th image was selected, normalised and down-sampled. (b). The images were multiplied by a mask function to prevent the image border and particles of dust from contributing to the alignment score. (c). The previously aligned image ("n") is used as a template and the images are correlated with one another: this is illustrated using red/green. The image to be aligned (n+5) is rotated and translated relative to the template (n) until a maximum correlation score is obtained (aligned). This newly aligned image is then used as a template to align the next image (n+10) and the process is repeated.

Image alignment

Every fifth image was selected. In cases where this section was missing or showed obvious defects such as folds, tears, compression or inadequate staining, the previous- or subsequent section was chosen. This produced five hundred and thirty five (535) images (representing 40 µm in the Z-direction), which were manually corrected in brightness and contrast using ImageJ Version 1.4.0. [83] and imported into Spider V.15 [84]. Images were normalised to a mean of 0 and standard deviation of 1 and down-sampled by a factor of 8 using bicubic interpolation to yield a sampling of 40 µm in X and Y (Fig. 1a). The images were then multiplied by a mask function representing a Gaussian falloff (Fig. 1b) and aligned to one another by maximising the cross-correlation function in X, Y and in-plane rotation (Fig. 1c) [12]. The resulting alignment was sufficient for resolving the parabronchi and larger blood vessels (Fig. 2) and permitted satisfactory reconstruction.
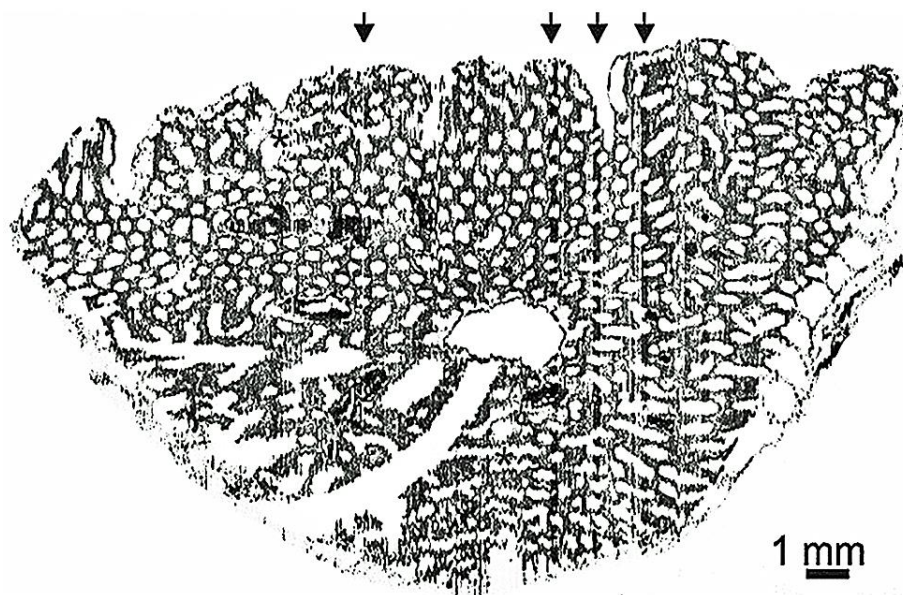
Figure 2: A cross-section (image 127) of the lung through the aligned image stack. All 535 individual sections can be seen as vertical lines. Errors in vertical alignment can be seen as "jitters" in individual structures. Areas where this is especially apparent are marked (*). Large differences in intensity between adjacent sections can be seen as vertical bands (arrows).

Segmentation of the reconstruction

To identify and segment the air-conducting elements of the reconstruction, an automated procedure was used. It involved applying a Gaussian filter and a threshold [12] [14]. In some cases, where the parabronchi were separated from adjacent ones by interparabronchial septa, a border was manually drawn around the periphery of the lung. Also, where two air-conducting elements lay adjacent to one another, to ascertain that they were resolved, lines were manually drawn between them. This process was iterated until a reasonable match between the unprocessed images and segmentation [85] was achieved (Fig. 3).

Blood vessel segmentation was achieved by manually defining the border of each blood vessel in the original (unprocessed) colour images (Fig. 3). These images were then down-sampled and aligned to one another by applying the alignment parameters obtained previously. To ensure that no blood vessels were mistaken for air-conducting elements

(especially those lacking erythrocytes in their lumen), the segmented blood vessels were subtracted from the air-conducting elements.

Reconstruction processing and display

The above procedure produced three image stacks: "air", "blood" and "original images". These were converted into volumes using Spider V.15 and low-pass Fourier filtered to a resolution of 160 µm with a Gaussian falloff [84] [85]. All three reconstructions were simultaneously displayed in UCSF Chimera 1.12 [86], the appropriate surface threshold value being determined by comparison with the "original images" volume. Larger blood vessels and airways were visualised by applying an additional low-pass Fourier filter to a resolution of 0.8 mm and adjusting the threshold value. The segmentation function in Chimera was used to further segment the blood vessels into arteries and veins.
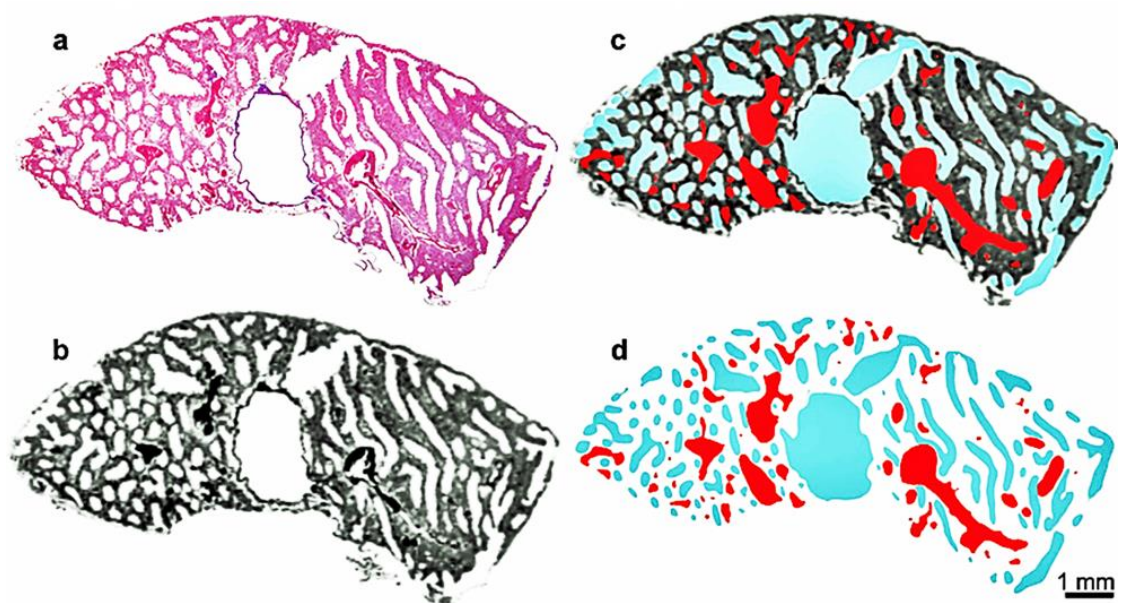
Figure 3: Segmentation of the reconstruction. (a). An unprocessed hematoxylin and eosin stained image (section 233) showing various air-conducting elements and blood vessels. (b). The same section shown in (a), but resampled, normalised and aligned. The larger vessels and lumina of the parabronchi are sufficiently well-resolved. (c). The manual blood vessel segmentation (red) and automated airways segmentation (cyan) superimposed on (b). An excellent match between the structures identifiable in the section was obtained. (d). The final image showing the airways (cyan) and blood vessels (red).

Results

Airways: bronchial system

The trachea divided into right- and left extrapulmonary primary bronchi (EPPB) at the syrinx. The EPPB penetrated the lung at the hilus where they lie craniolateral to the pulmonary artery (PA) and caudomedial to the pulmonary vein (PV). On entering the lung, the EPPB becomes the intrapulmonary primary bronchus (IPPB) or the mesobronchus which changes in diameter and course as it passes through the lung to exit the lung at the abdominal air sac. On the various aspects of its lumen, as it passes through the lung, the IPPB gives off four sets of secondary bronchi. These are: the medioventral secondary bronchi (MVSB) that originate from the dorsomedial aspect of the lumen; the mediodorsal secondary bronchi (MDSB) that arise from the dorsal wall; the lateroventral secondary bronchi (LDSB) that arise from the caudoventral part and; the laterodorsal secondary bronchi (LDSB) that emanate from the

lateral aspect of the distal part of the IPPB. The parabronchi or the tertiary bronchi interconnect the secondary bronchi. The parabronchial system, which connects the MVSB to the MDSB, forms the paleopulmo or the 'old lung' while those which connect the MDSB to the LVSB and the LDSB form the neopulmo or the 'new lung'. The paleopulmonic parabronchi form a stack or pile of air conduits which largely occupy the dorsocranial part of the lung while the neopulmonic ones are mostly located on the caudoventral part of the lung. As they (paleopulmonic parabronchi) join the MVSB to the MDSB on the dorsal aspect of the lung, they form hoop-like shapes: the paleopulmonic parabronchi lie parallel to each other and sporadically anastomose with each other while the neopulmonic parabronchi anastomose profusely, forming a dense network. Generally, the paleopulmonic parabronchi are larger in size compared to the neopulmonic ones.

Vascular systems: pulmonary artery (PA)
The PA enters the hilus ventral to the root of the first MVSB. On penetrating the lung, it divides into four main branches (= rami), namely the accessory-, the cranial-, the caudomedial- and the caudolateral branches. The branches supply blood to different parts of the lung: the accessory branch, which is the first blood vessel to arise from the PA, supplies blood to a small part of the lung ventral to hilus; the cranial branch supplies blood to the craniodorsal region of the lung cranial to the second costal sulcus; the caudolateral branch supplies blood to the ventrolateral part of the lung and; the caudomedial branch, which is the most direct extension of the PA, supplies blood to most of the lung caudal to the second costal sulcus. The four branches of the PA divide the lung roughly into a cranial- and a caudal arterial vascular region, with a vertical transverse line passing through the second costal sulcus forming the anatomical landmark or the dividing boundary: the cranial part of the lung is supplied with blood by the accessory- and the cranial branches while the caudal one is supplied by the caudomedial- and the caudolateral branches. Along the median longitudinal plane which divides the lung into a lateral and a medial half along the so-called *linea anastomotica*, i.e., the area marking connection between the parabronchi from the MVSB and those from the MDSB (the paleopulmonic parabronchi) meet, the former part of the lung is supplied by the caudolateral branch of the PA while the later one is supplied by the caudomedial branch. In this study, up to about the level of the interparabronchial arteries, no anastomoses were observed between the four branches of the PA.

Vascular system: pulmonary vein (PV)
At the hilus, the PV is separated from the PA by the intrapulmonary primary bronchus. The PV is formed by connection of three converging blood vessels (radices), namely the cranial-, the caudal- and the ventral radices. The radices join outside the lung to form the PV. In our study, the connection of the radices was not included in the 3-D reconstruction because that part of the lung was inadvertently cut off during trimming off of adhering connective tissue. Most of the craniodorsal part of the lung is drained by the cranial radix which is formed by confluence of three large veins; the caudal radix drains the part of the lung caudal to the third costal sulcus and is formed by as many as four radices which extend dorsally and ventrally and; the ventral radix, which drains the cranioventral part of the lung comprises two main branches which drain the part of the lung located between the second and the third costal sulci. Up to the level of the interparabronchial veins, no anastomoses were observed between the radices.

Discussion

Employing different methods, the morphologies of the airways of the avian lung have been investigated by various investigators [64]-[66] [71] [87]-[90]. Consensus on the numbers of

airways, their shapes, connections, topographic locations and nomenclature has, however, not yet been reached [74. While interspecific differences have been reported [64]-[66] [68] [71] [91] [92], it cannot be completely ruled out that interspecimen differences occur largely from developmental abnormalities and irregularities and the environmental conditions under which the avian eggs are incubated. In this study, in addition to 3-D reconstruction of the airways- and the blood vessels, for more insightful visualization of the morphologies and the spatial associations between the different parts, movies which allowed the rotation of the constructions across different planes and extraction (removal) and re-introduction of the different parts to the constructions were prepared. Although certain weaknesses exist in all the techniques which have been used to study the morphology of the avian lung, this study corroborates most of the previous accounts. Indisputably, 3-D reconstruction is a very powerful means of studying the morphologies of biological structures, including those of structurally complex avian respiratory system.

The pulmonary vasculature of birds has been studied by [93]-[98]. Various techniques which included injection with markers and following the paths they follow, e.g., microspheres, in the blood vessels by light microscopic examination and microfilm, silicone, mercox or latex rubber injection followed by maceration and preparation of casts or replicas have been used. While our observations generally agree with those previously made by other investigators, certain differences exist. Unlike in the mammalian lung where arteries closely follow airways while veins run intersegmentally [99] [100], i.e., they are located between the airways and the arteries, in the avian lung, the airway- and the vascular systems do not display such arrangement. This may be explained by the complex development of the avian lung [101]-[103], where, in lungs of phylogenetically derived species (evolutionarily advanced birds), the paleopulmonic part develops first to be followed by the neopulmonic one [102] [103]: the adult lungs of an evolutionarily developed bird comprises two distinctive parts, namely the 'paleopulmo' and the 'neopulmo' which display structural and functional differences: the two regions are typically located in different regions of the lung [64] [68] [92] and the two parts are ventilated differently. The paleopulmo is continuously and unidirectionally ventilated in a caudocranial direction by concerted actions of the air sacs [67] [104] while the neopulmo is ventilated tidally, i.e., back-and-forward. Taking these properties into consideration, it is axiomatic that the airways and the blood vessels of the avian lung cannot follow each other in the same way as in the mammalian lung, where mesenchymal cells which contribute to the development of the airways and the blood vessels start at the same point (essentially the lung bud) and in close proximity grow outwards as the lungs develop [105]-[107], forming the various functional systems. Regarding the observations of [93] [94], in comparison with the observations noted in this study, certain structural discrepancies exist. The main ones are: a) while two main radices were reported to converge and form the PV [93] [94], here, three main blood vessels drained the lung and joined to form the PV and; b) the second costal sulcus and not the third one formed the boundary between the cranial- and the caudal blood supply- and the respective drainage regions of the lung by the PA and PV, respectively.

In conclusion, compared to the other techniques which have hitherto been employed to study the morphology of the airway- and the vascular systems of the avian lung, incontrovertibly, 3-D reconstruction is the more robust technique. When it is combined with preparation of movies which can be operated and closely viewed from different angles, the geometries of the structures can be thoroughly scrutinized and understood. It is important to underscore that while a powerful technique in its own right, scanning electron microscopy (SEM), which is conventionally applied for imaging biological structures, does not strictly generate 3-D images as generally wrongly interpreted: although they may appear so, the resulting images

do not have an aspect of depth. Presently, there are several SEM techniques that can be used to obtain 3-D information on a biological sample [108]-[110]. Some of them can be done on any microscope and some require specialist instrumentation, software, or microscopes.

Acknowledgements

References

[1] Miranda, K., Girard-Dias, W., Attias, M., de Souza, W. and Ramos, I. (2015) Three dimensional reconstruction by electron microscopy in the life sciences: an introduction for cell and tissue biologists. *Molecular Reproduction and Development* **82**, 530-547.

[2] Darwin, C. (1859) *On the Origin of Species by Means of Natural Selection, or the Preservation of Favoured Races in the Struggle for Life*. John Murry, London.

[3] Nachtigall, W. (1997) *Exploring with the Microscope: A Book of Discovery and Learning*. Sterling Publications, London.

[4] Savile, B. and Bracegirdle, B. (1998) *Introduction to Light Microscopy*. Springer-Verlag, New York.

[5] His, W. (1880) *Anatomie menschlicher Embryonen*. Vogel, Leipzig.

[6] Kastschenko, N. (1886) Methode zur genauen rekonstruktion kleinerer makroskopischer gegenstande. *Archive für Anatomie und Physiologie Abteilung* **1**, 388-394.

[7] Odhner, T. (1911) Zum naturlichen System der digenen Trematoden IV. *Zoologischer Anzeiger.* **38**, 513-531.

[8] Ohta, Y. and Millhouse, E.W., Glass Plate Reconstruction from Serial Sections Used in the Study of Neonatal Biliary Atresia, *Stereology*, Elias H. Ed.. Springer, Berlin, 1967, 302-303.

[9] Ward, S., Thomson, N., White, J.G. and Brenner, S. (1975) Electron microscopical reconstruction of the anterior sensory anatomy of the nematode, *Caenorhabditis elegans*. *Journal of Comparative Neurology* **160**, 313-337.

[10] Teutsch, H.F., Schuerfeld, D. and Groezinger, E. (199) Three-dimensional reconstruction of parenchymal units in the liver of the rat. *Hepatology* **29**, 494-505.

[11] Woodward, J.D. and Maina, J.N. (2005) A 3D digital reconstruction of the components of the gas exchange tissue of the lung of the muscovy duck, *Cairina moschata*. *Journal of Anatomy* **206**, 477-492.

[12] Woodward, J.D. and Maina, J.N. (2008) Study of the structure of the air- and blood capillaries of the gas exchange tissue of the avian lung by serial section three-dimensional reconstruction. *Journal of Microscopy* **230**, 84-93.

[13] Song, W.C., Hu, K.S., Kim, H.J. and Koh, K.S. (2007) A study of the secretion mechanism of the sebaceous gland using three-dimensional reconstruction to examine the morphological relationship between the sebaceous gland and the arrector pili muscle in the follicular unit. *British Journal of Dermatology* **157**, 325-330.

[14] Maina, J.N. and Woodward, J.D. (2009) Three-dimensional serial section computer reconstruction of the arrangement of the structural components of the parabronchus of the ostrich, *Struthio camelus* lung. *Anatomical Record* **292**, 1685-1698.

[15] Sun, K., Zhang, J., Chen, T., Chen, Z., Chen, Z., Li, Z., Li, H. and Hu, P. (2009) Three dimensional reconstruction and visualization of the median nerve from serial tissue sections. *Microsurgery* **29**, 573-577.

[16] Penczek, P.A. (2010) Fundamentals of three-dimensional reconstruction from projections. *Methods in Enzymology* **482**, 1-33.

[17] Wu, X., Yu, Z. and Liu, N. (2012) Comparison of approaches for microscopic imaging of skin lymphatic vessels. *Scanning* **34**, 174-180.

[18] Onozato, M.L., Klepeis, V.E, Yagi, Y. and Mino-Kenudson, M. (2012) A role of three-dimensional (3D)-reconstruction in the classification of lung adenocarcinoma. *Analytical Cellular Pathology* **35**, 79-84.

[19] Baghaie, A., Pahlavan, Tafti, A., Owen, H.A., D'Souza, R.M. and Yu, Z. (2017) Three-dimensional reconstruction of highly complex microscopic samples using scanning electron microscopy and optical flow estimation. *PLoS One* **12(4)**, e0175078.

[20] Chozinski, T.J., Mao, C., Halpern, A.R., Pippin, J.W., Shankland, S.J., Alpers, C.E., Najafian, R. and Vaughan, J.G. (2018) Volumetric, nanoscale optical imaging of mouse and human kidney via expansion microscopy. *Scientific Reports* **8,** 10396.

[21] Kartasalo, K., Latonen, L., Vihinen, J., Visakorpi1, T., Nykter, M. and Ruusuvuori1, P. (2018) Comparative analysis of tissue reconstruction algorithms for 3D histology. *Bioinformatics* **34**, 3013-3021.

[22] Lorenz, U.J. and Zewail, A. (2014) Observing liquid flow in nanotubes by 4D electron microscopy. *Science* **344**, 1496-1500.

[23] Bissell, M.J. (2017) Goodbye flat biology - time for the 3rd and the 4th dimensions. *Journal of Cell Science* **130**, 3-5.

[24] Turing, A.M. (1952) The chemical basis of morphogenesis. *Philosophical Transactions of the Royal Society (London) B* **237**, 37-72.

[25] French, R. (1988) *Invention and Evolution Design in Nature and Engineering*. Cambridge University Press, Cambridge.

[26] Rowley, M.J. and Corces, V.G. (2018) Organizational principles of 3D genome architecture. *Nature Reviews Genetics* **19**, 789-799.

[27] Rowley, M.J., Nichols, M.H., Lyu, X., Ando-Kuri, M., Rivera, S.M., Hermetz, K., Wang, P., Ruan, Y. and Corces, V.G. (2017) Evolutionarily conserved principles predict 3D chromatin organization. *Molecular Cell* **67**, 837-852.

[28] Duan, Z. and Blau, C.A. (2012) The genome in space and time: does form always follow function? How does the spatial and temporal organization of a eukaryotic genome reflect and influence its function? *Bioessays* 34, 800-810.

[29] Ravi, M., Paramesh, V., Kaviya, S.R., Anuradha, E. and Solomon, P.F.D. (2015) 3D cell Culture systems: advantages and applications. *Journal of Cell Physiology* **230**, 16-26.

[30] Cavo, M., Fato, M., Peñuela, L., Beltrame, F., Raiteri, R. and Scaglione, S. (2016) Microenvironment complexity and matrix stiffness regulate breast cancer cell activity in a 3D *in vitro* model. *Scientific Reports* **6:35367**. doi:10.1038/srep35367.

[31] Powell, K. (2017) Adding depth to sell culture. *Science Technology Feature* **361, 6402**.

[32] Zanoni, M., Piccinini, F., Arienti, C., Zamagni, A., Santi, S., Polico, R., Bevilacqua, A. and Tesei, A. (2016) 3D tumor spheroid models for *in vitro* therapeutic screening: a systematic approach to enhance the biological relevance of data obtained. *Scientific Report* **6:19103**. doi: 10.1038/srep19103

[33] Baker, B.M. and Chen, C.S. (2012) Deconstructing the third dimension – how 3D culture microenvironments alter cellular cues. *Journal of Cell Science* **125**, 3015-3024.

[34] Fang, Y. and Eglen, R. (2017) Three-dimensional cell cultures in drug discovery and development. *SLAS Discovery: Advancing Life Sciences* **22**, 456-472.

[35] Langhans, S. (2018) Three-dimensional *in vitro* cell culture models in drug discovery and drug repositioning. *Fronteers in Pharmacology* **22**, 456-472.

[36] Edmondson, R., Broglie, J., Adcock, A. and Yang, L. (2014) Three-dimensional cell culture systems and their applications in drug discovery and cell-based biosensors. *Assay Drug Development Technology* **12**, 207- 218.

[37] Lee, G.Y., Kenny, P.A., Lee, E.H. and Bissell, M.J. (2007) Three–dimensional culture models of normal and malignant breast epithelial cells. *Nature Methods* **4**, 359-365.

[38] Abbot, A. (2003) Biology's new dimension. *Nature* **424**, 870-872.

[39] Glauco, S. (2010) Three-dimensional tissue culture based on magnetic cell levitation. *Nature Nanotechnology* **5**, 291-296.

[40] Haycock, J.W. (2011) 3D cell culture: a review of current approaches and techniques. *Methods in Molecular Biology* **695**, 1-15.

[41] Derricott, H., Luu, L., Fong, W.Y., Hartley, C.S., Johnston, L.J., Armstrong, S.D., Randle, N., Duckworth, C.A., Campbell, B.J., Wastling, J.M., Coombes, J.L. (2019) Developing a 3D intestinal epithelium model for livestock species. *Cell and Tissue Research* 375, 409-424.

[42] Levinthal, C. and Ware, R. (19772) Three-dimensional reconstruction from serial sections. *Nature* **236**: 207-209.

[43] Perkins, W.J. and Green, R.J. (1982) Three-dimensional reconstruction of biological sections. *Journal of Biomedical Engineering* **4**, 37-43.

[44] Latamore, G.B. (1983) Creating 3-D models for medical research. *Computer Graphics World* **5**, 31-38.

[45] Mercer, R.R. and Crapo, J.D. Structure of the Gas Exchange Region of the Lungs Determined by Three Dimensional Reconstructions, *Toxicology of the Lung*, Gardner, D.E., Crapo, J.D., Massaro, E.J. Eds.. Raven Press, New York, 1988, 43-70.

[46] Anderson, J.R., Wilcox, M.J., Wade, P.R. and Barrett, S.F. (2003) Segmentation and 3D reconstruction of biological cells from serial slice images. *Biomedical Science Instrumentation* **39**,117-122.

[47] Rosenhain, S., Magnuska, Z.A., Yamoah, G.G., Rawashdeh, W.A., Kiessling, F. and Gremse, F. (2018) A preclinical micro-computed tomography database including 3D whole body organ segmentations. *Scientific Data* **5**. Article number 180294.

[48] Vints, K., Vandael, D., Baatsen, P., Pavie, B., Vernaillen, F., Corthout, N., Rybakin, V., Munck, S. and Gounko, N.V. (2019) Modernization of Golgi staining techniques for high-resolution, 3-dimensional imaging of individual neurons. *Scientific Reports* **9**. Article number: 130.

[49] Herman, G. T. (2009) *Fundamentals of Computerized Tomography: Image Reconstruction from Projection, 2nd Edition*. Springer-Verlag, Berlin.

[50] Handschuh, S., Schwaha, T. and Metscher, B. D. (2010) Showing their true colors: a practical approach to volume rendering from serial sections. *BMC Developmental Biology* **10**, 41.

[51] Wang, C.W., Gosno, E.B. and Li, YS (2015a) Fully automatic and robust 3D registration of serial-section microscopic images. *Scientific Reports* **5, 15051**. Doi 10.1038/srep15051.

[52] Wang, Y., Xu, R., Luo, G. and Wu, J. (2015b) Three-dimensional reconstruction of light microscopy image sections: present and future. *Frontiers of Medicine* **9**, 30-45.

[53] Born, G. (1883) Die Plattenmodelliermethode. *Archives fur mikroskopie Anatomie* **22**, 584-599.

[54] Strasser, H. (1886) Ueber das Studium der Schnittserien und über die Hülfsmittel, welche die Reconstruction der zerlegten Form erleichtern. *Zeitschrifft Wissen Mikroskope* **3**, 179-195.

[55] Strasser, H. (1987) Ueber die Methoden der plastischen Rekonstruktion. *Zeittschrift Wissen Mikroskope* **4**,168-208.

[56] Weninger, W.J. and Mohun, T. (2002) Phenotyping transgenic embryos: a rapid 3-D screening method based on episcopic fluorescence image capturing. *Nature Genetics* **30**, 59-65.

[57] Ewald, A.J., McBride, H., Reddington, M., Fraser, S.E., Kerschmann, R. (2002) Surface imaging microscopy, an automated method for visualizing whole embryo samples in three dimensions at high resolution. *Developmental Dynamics* **225**, 369-375

[58] Liu, B., Gao, X.L., Yin, H.X., Luo, S.Q. and Lu, J. (2007) A detailed 3D model of the guinea pig cochlea. *Brain Structure and Function* **212**, 223-230.

[59] Rau, T.S., Hussong, A., Herzog, A., Majdani, O., Lenarz, T. and Leinung, M. (2011) Accuracy of Computer aided geometric 3D reconstruction based on histological serial microgrinding preparation. *Computational Methods Biomechanicaland Biomedical Engineering* **14**, 581-594.

[60] Carletti, E., Motta, A. and Migliaresi, C. (2011) Scaffolds for tissue engineering and 3D cell culture. *Methods in Molecular Biology* **695**, 17-39.

[61] Deluzio, TGB, Seifu, D.G.and Mequanint, K. (2011) 3D scaffolds in tissue engineering and regenerative medicine: beyond structural templates? *Pharmaceutical Bioprocessing* **1**, 267-281

[62] Yu, Y., Moncal, K.K., Li, J., Peng, W., Rivero, I., Martin, J.A. and Ozbolat, I.T. (2016) Three-dimensional bioprinting using self-assembling scalable scaffold-free tissue strands as a new biolink. *Scientific Reports* **6**:28714. doi: 10.1038/srep28714.

[63] Jensen, G., Morrill, C. and Huang, Y. (2018) 3D tissue engineering, an emerging technique for pharmaceutical research. *Acta Pharmaceutica Sinica B* **8**, 756-766.

[64] Duncker, H.R. (1971) The lung-air sac system of birds. A contribution to the functional anatomy of the respiratory apparatus. *Ergebinisse Anatomie Entwicklungsgeschichte* **45**, 1-171.

[65] Duncker, H-R. (1972) Structure of avian lungs. *Respiration Physiology* **14**, 44-63.

[66] Duncker, H-R. (1974) Structure of avian respiratory tract. *Respiration Physiology* **22**, 1-19.

[67] Scheid, P. (1979) Mechanisms of gas exchange in bird lungs. *Review of Physiology Biochemistry and Pharmacology* **86**, 137-186.

[68] McLelland, J., Anatomy of the Lungs and Air Sacs, *Form and Function in Birds, Vol. IV*, King, A.S., McLelland, J. Eds.. Academic Press, London, 1989, 221-279.

[69] Powell, F.L., Respiration, *Sturkie's Avian Physiology, 5ᵗʰ Edition*, Whittow, G.C. Ed.. San Diego, Academic Press, 2000, 233-264.

[70] Powell, F.L. and Hopkins, S.R. (2004) Comparative physiology of lung complexity: implications for gas exchange. *News in Physiological Science* **19**, 55-60.

[71] Maina, J.N. (2005) *The Lung Air Sac System of Birds: Development, Structure, and Function*. Springer-Verlag, Heidelberg.

[72] Harvey, E.P. and Ben-Tal, A. (2015) Robust unidirectional airflow through avian lungs: new insights from a piecewise linear mathematical mode. *PLoS Computational Biology* **12(2),** e1004637.

[73] Coiter, V., Anatomie Avium, *Externum et Internarum Praecipalium Humani Corporis Partium Tabulae atque Anatomicae Exercitationes Observationesque Varieae*. Norimbergae, Germany, 1573, 130-133.

[74] Maina, J.N. (2017) Pivotal debates and controversies on the structure and function of the avian respiratory system: setting the record straight. *Biological Reviews* **92,** 1475-1504.

[75] Maina, J.N., Singh, P. and Moss, E.A. (2009) Inspiratory aerodynamic valving occurs in the ostrich, *Struthio camelus* lung: computational fluid dynamics study under resting unsteady state inhalation. *Respiration Physiology and Neurobiology* **169**, 262-270.

[76] Maina, J.N., The Morphometry of the Avian Lung, *Form and Function in Birds, Vol. 4*, King, A.S., McLelland, J. Eds.. Academic Press, London, 1989, 307-368.

[77] Maina, J.N., King, A.S. and Settle, J.G. (1989) An allometric study of the pulmonary morphometric parameters in birds, with mammalian comparison. *Philosophical Transactions of the Royal Society (London) B* **326**, 1-57.

[78] Maina, J.N., McCracken, K.G., Chua, B., York, J.M. and Milsom, W.K. (2017) Morphological and morphometric specializations of the lung of the Andean goose, *Chloephaga melanoptera*: a lifelong high-altitude resident. *PLoS One* **12(3)**: e0174395.

[79] Maina, J.N. (2000) What it takes to fly: The novel respiratory structural and functional adaptations in birds and bats. *Journal of Experimental Biology* **203**, 3045-3064.

[80] Tucker, V.A., Energetics of natural avian flight. *Avian Energetics*, Paynter, R.A. Ed.. Nuttal Ornithological Club, Cambridge (MA), 1974, 298-333.

[81] Altshuler, D.L. and Dudley, R. (2006) The physiology and biomechanics of avian flight at high altitude. *Integrative Comparative Biology* **46**, 4-8.

[82] Scott, G.R. (2011) Elevated performance: the unique physiology of birds that fly at high altitudes. *Journal of Experimental Biology* **214**, 2455-2462.

[83] Rueden, C.T., Schindelin, J., Hiner, M.C., DeZonia, B.E., Walter, A.E., Arena, E.T. and Eliceiri, K.W. (2017) ImageJ2: ImageJ for the next generation of scientific image data. *BMCBioinfornatics* **18**, 529.

[84] Frank, J., Radermacher, M., Pencze, P., Zhu, J., Li, Y., Ladjadj, M. and Leith, A. (1996) SPIDER and WEB: Processing and visualization of images in 3D electron microscopy and related fields. *Journal of Structural Biology* **116**, 190-199.

[85] Pintilie, G.D., Zhang, J., Goddard, T.D., Chiu, W. and Gossard, D.C. (2010) Quantitative analysis of cryo-EM density map segmentation by watershed and scale-space filtering, and fitting of structures by alignment to regions. *Journal of Structural Biology* **170**, 427-38.

[86] Pattersen, E.F., Goddard, T.D., Huang, C.C., Couch, G.S., Greenblatt, D.M., Meng, E.C. and Ferrin, T.E. (2004) UCSF Chimera - a visualization system for exploratory research and analysis. *Journal of Computational Chemistry* **25**, 1605-1612.

[87] Makanya, A.N. and Djonov, V. (2008) Development and spatial organization of the air conduits in the lung of the domestic fowl, *Gallus* variant *domesticus*. *Microscopic Research Techniques* **71**, 689-702.

[88] Makanya, A.N. and Djonov, V. (2009) Parabronchial angioarchitecture in developing and adult chickens. *Journal of Applied Physiology* **106**, 1959-69.

[89] Makanya, A.N., Kavoi, B.M., Djonov, V. (2014) Three-dimensional structure and disposition of the air conducting and gas exchange conduits of the avian lung: the domestic duck (*Cairina moschata*). *Journal of Anatomy* **1**, 1-9.

[90] Pandey, A.K., Praveen, P.K., Ganguly, S., Para, P.A., Wakchaure, R., Saroj and Mahajan, T. (2015) Avian respiratory and physiology with its interspecies variations: A review. *World Journal of Pharmacology and Life Sciences* **1**, 137-148.

[91] West, N.H., Bamford, O.S. and Jones, D.R. (1977) A scanning electron microscope study of the microvasculature of the avian lung. *Cell Tissue Research* **176**, 553-564.

[92] King, A.S. (1966) Structural and functional aspects of the avian lung and its air sacs. *International Journal of Reviews in General Experimental Zoology* **2**, 171-267.

[93] Abdalla, M.A. and King, A.S. (1975) The functional anatomy of the pulmonary circulation of the domestic fowl. *Respiration Physiology* **23**, 267-290.

[94] Abdalla, M.A., The Blood Supply to the Lung, *Form and Function in Birds, Vol. 4*, King, A.S., McLelland, J., Eds.. Academic Press, San Diego, 1989, 281-306.

[95] Radu, C. and Radu, L. (1971) Le dispositive vasculaire du poumon chez les oiseaux domestiques. *Revue de Medecine Veterinaire* **122**, 1219-1226.

[96] Abdalla, M.A. and King, A.S. (1976a) Pulmonary arteriovenous anastomoses in the avian lung: do they exist. *Respiration Physio*logy **27**, 187-191.

[97] Abdalla, M.A and King, A.S. (1976b) The functional anatomy of the bronchial circulation of the domestic fowl. *Journal of Anatomy* **121**, 537-550.

[98] Abdalla, M.A. and King, A.S. (1977) The avian bronchial arteries: species variations. *Journal of Anatomy* **123**, 697-704.

[99] Weibel, E.R. (1984) *The Pathway for Oxygen: Structure and Function in the Mammalian Respiratory System*. Harvard University Press, Cambridge (MA).

[100] Hislop, A.A. (2002) Airway and blood vessel interaction during lung development. *Journal of Anatomy*

[101] Duncker, H-R., Development of the Avian Respiratory and Circulatory Systems, *Respiratory Function in Birds, Adult and Embryonic*, Ducker, H.R. Ed.. Springer-Verlag, Berlin, 1978, 260-273.

[102] Maina, J.N. (2003a) A systematic study of the development of the airway (bronchial) system of the avian lung from days 3 to 26 of embryogenesis: a transmission electron microscopic study of the domestic fowl, *Gallus gallus* variant *domesticus*. *Tissue and Cell* **35**, 375-391.

[103] Maina, J.N. (2003b) Developmental dynamics of the bronchial- (airway) and air sac systems of the avian respiratory system from days 3 to 26 of life: a scanning electron microscopic study of the domestic fowl, *Gallus gallus* variant *domesticus*. *Anatomy and Embryology* **207**, 119-134. **201**, 325-334.

[104] Fedde, R. (1980 The structure and gas flow pattern in the avian lung. *Poultry Science* **59**, 2642-2653.

[105] Schittny, J.N. and Burri, P.H. Development and Growth of the Lung, *Fishman's Pulmonary Disorders and Diseases, 4th edition*, Fishman, A.P. Ed., McGraw Hill, New York, 2008, 91-114.

[106] Burri, P.H. (1984) Fetal and postnatal development of the lung. *Annual Review of Physiology* **46**, 617-628.

[107] Burri, P.H., Development and Growth of the Human Lung, *Handbook of Physiology, Section 3: The Respiratory System*, Fishman, A.P., Fisher, A.B. Eds.. American Physiological Society, Bethesda (MD), 1985, 1-46.

[108] Hughes, L.C., Archer, C.W. and Gwynn, I. (2005) The ultrastructure of mouse articular cartilage: collagen orientation and implications for tissue functionality. A polarised light and scanning electron microscope study and review. *European Cells and Materials* **9**, 68-84.

[109] Peddie, C.J. and Collinson, L.M. (2014) Exploring the third dimension: volume electron microscopy comes of age. *Micron* **61**, 9-19.

[110] Woodward, J.D., Wepf, R. and Sewell, B.T. (2009) Three-dimensional reconstruction of biological macromolecular complexes from in-lens scanning electronmicro-graphs. *Journal of Microscopy* **234**, 287-292.